Indicial lift response function: an empirical relation for finitethickness airfoils, and effects on aeroelastic simulations

Bergami, Leonardo; Gaunaa, Mac; Heinz, Joachim Christian

Published in:
Wind Energy

Link to article, DOI:
10.1002/we.1516

Publication date:
2013

Document Version
Early version, also known as pre-print

Indicial lift response function: an empirical relation for finite-thickness airfoils, and effects on aeroelastic simulations

Leonardo Bergami, Mac Gaunaa, and Joachim Heinz
Technical University of Denmark, Wind Energy Department, Roskilde, 4000 Denmark
leob@dtu.dk

This is the accepted version of the following article: Bergami, Leonardo, Gaunaa, Mac and Joachim Heinz. "Indicial lift response function: an empirical relation for finite-thickness airfoils, and effects on aeroelastic simulations." *Wind Energy* 16, no. 5 (2014):681-93. doi:10.1002/we.1516, which has been published in final form at Wiley Online Library

Abstract

The aeroelastic response of wind turbines is often simulated in the time domain using indicial response techniques. Unsteady aerodynamics in attached flow are usually based on Jones's approximation of the flat plate indicial response, although the response for finite-thickness airfoils differs from the flat plate one.

The indicial lift response of finite-thickness airfoils is simulated with a panel code, and an empirical relation is outlined connecting the airfoil indicial response to its geometric characteristics. The effects of different indicial approximations are evaluated on a 2D profile undergoing harmonic pitching motion in the attached flow region; the resulting lift forces are compared to Computational Fluid Dynamics (CFD) simulations. The relevance for aeroelastic simulations of a wind turbine is also evaluated, and the effects are quantified in terms of variations of equivalent fatigue loads, ultimate loads, and stability limits.

The agreement with CFD computations of a 2D profile in harmonic motion is improved by the indicial function accounting for the finite-thickness of the airfoil. Concerning the full wind turbine aeroelastic behavior, the differences between simulations based on Jones's and finite-thickness indicial response functions are rather small; Jones's flat-plate approximation results in only slightly larger fatigue and ultimate loads, and lower stability limits.

1 Introduction

Aeroelastic simulation tools require aerodynamic models accounting for unsteady aerodynamic effects. The aerodynamic model should be computationally light, as to limit the resources required in time marching simulations, but, at the same time, complex enough to predict with sufficient accuracy the aerodynamic loads arising on the blade, both in attached, and separated (stalled) flow conditions.

A large contribution to the total aerodynamic loading is generated on the outer sections of the blades, which, in modern wind turbines, operate most of the time in attached flow conditions. Unsteady aerodynamic forces in attached flow are frequently described in the time domain using indicial formulations, as described by Beddoes [1] and Leishman [2]. Wind turbine simulation tools based on this approach include, among others, the aeroelastic code HAWC2[3, 4], Bladed [5], and FAST[6, 7].

The unsteady lift force in attached flow is described, following Theodorsen's theory [8], as the sum of two contributions: a non-circulatory and a circulatory one. The non-circulatory lift, or added mass term, represents the lift force that would arise on the airfoil in a non-circulatory flow due to the reaction of the fluid accelerated with the airfoil motion; the non-circulatory term has no dependency on time, and only depends on the instantaneous acceleration of the fluid around the airfoil. The circulatory lift, on the contrary, carries a memory effect, which originates from the vorticity shed into the wake to compensate the change of circulation around the airfoil, as governed by Kelvin's theorem on conservation of circulation [9].

The circulatory lift for an airfoil undergoing arbitrary motion is computed in the time domain applying Duhamel's superposition integral of indicial step responses [9]:

$$L_c = 2\pi\rho U b \left[w_{3/4}(0) \cdot \Phi(\tau) + \int_0^\tau \frac{\mathrm{d}w_{3/4}}{\mathrm{d}\sigma} \Phi(\tau - \sigma) \mathrm{d}\sigma \right]. \tag{1}$$

Where, b is the half-chord length, $w_{3/4}$ is the downwash at the three-quarters chord, and the dimensionless variable τ expresses the time dependency, as the distance in half-chords traveled by the airfoil:

$$\tau = \frac{Ut}{b}. \tag{2}$$

The indicial response function $\Phi(\tau)$ represents the ratio between the actual unsteady circulatory lift, and the corresponding steady value, following a unit step change in the quasi-steady loading. Wagner[9] determines the indicial response for a flat plate in incompressible flow as a function that tends asymptotically to unity, and starts from a value of 0.5 at $\tau = 0$, indicating that half the change in circulatory lift is obtained at the initial instant, figure 3. Wagner's function is not formulated in simple analytical terms, rendering Duhamel's integration rather complex; to obviate the problem, the response function is approximated as a linear combination of exponential terms [9]:

$$\Phi \approx 1 - \sum_{i=1}^{N_{\text{terms}}} A_i \exp^{b_i \tau}; \tag{3}$$

The exponential form of the response function allows for a very efficient numerical integration of Duhamel's expression. In fact, Duhamel's integral, eq. (1), at time $t + \Delta t$ can be then evaluated as the sum of a decay, and an increment term; the decay term depends on the integral value at the previous time step t, while the increment term only includes an integration from time t to $t + \Delta t$, thus avoiding to perform integration from the time origin $t = 0$ at every new time step [9].

Using the exponential form of the indicial lift response function, Jones[10] proposes a two terms approximation for the flat plate indicial response(figure 3):

$$\Phi = 1 - 0.165 \exp^{-0.045\tau} - 0.335 \exp^{-0.3\tau} . \tag{4}$$

Several references report indicial lift responses for airfoils with finite thickness that differ from the flat plate response. Giesing[11] shows indicial curves below the flat plate one for the response of Von Mises and Jukowsky airfoils; similar results are obtained by Basu and Hancock[12], who simulate the step response of a Von Mises airfoil with a panel code. Chow[13] concludes that finite thickness airfoils have a slower step response, and the response speed decreases as the airfoil thickness and trailing edge angle are augmented.

More recently, Gaunaa [14] applies a panel code method to compute the response of NACA symmetric airfoils with different thicknesses, and shows that the response curve tends to the flat plate one as the thickness is reduced. In Hansen et al. [4], the same panel code method is used to simulate the step response of a 24% thick airfoil; the resulting indicial response is approximated by a two term exponential function which is then supplied to the Beddoes-Leishman model described in the report. Hansen et al. show that, for an airfoil undergoing harmonic pitch variations, the unsteady lift force based on the finite-thickness response is in better agreement with CFD simulations.

Nevertheless, Jones's approximation for the flat plate response remains a widespread standard in incompressible attached flow models, and, to the authors' knowledge, no investigations evaluating the effects that different indicial response approximations would cause on wind turbine aeroelastic simulations are reported in literature.

The present work proposes an empirical function relating the geometric characteristics of an airfoil to its indicial lift response. Gaunaa's[14] panel code is used to compute the indicial response for a set of airfoils with different geometries; the indicial response curves are approximated with Jones-like two-term exponential functions, in the form of eq. (3). The different airfoils and corresponding indicial responses provides the dataset on which regression methods are applied to outline the empirical function, which is then tested on airfoils outside the dataset.

The effects of modified lift response functions are investigated for an airfoil undergoing harmonic pitching motion, and the resulting unsteady lift histories are compared to CFD simulations. The consequences on aeroelastic computations for a full wind turbine are evaluated by running time marching simulations of the NREL 5-MW baseline turbine [15] with the aeroelastic tool HAWC2 [3].

The method described in this article builds on the work presented by Gaunaa et al. [16] at the 49th AIAA-ASME conference. Compared to the preliminary results reported in the conference paper [16], the present article broadens the analysis on how changes in the indicial lift function affects aeroelastic loads simulations, and also includes an investigation on the effects on stability limits prediction.

2 Model and method

In order to estimate the effects that each airfoil geometry has on the indicial lift response function, several airfoil profile shapes have been considered. Each airfoil profile is discretized into panels, and the circulatory indicial lift response is simulated using a panel code. The simulated indicial lift response is fitted with a two term exponential function, and an empirical relation is sought in order to link the coefficients defining the exponential indicial response function (A_1,A_2,b_1,b_2, eq. (3)) to the airfoil geometric characteristics.

2.1 Airfoil profiles

A preliminary investigation considered airfoil shapes taken from the modified NACA 4-digits family[17]. The profiles have a simple geometry, which is obtained as a superposition of thickness distribution to the airfoil mean line, and it is fully described by a set of five parameters. [1]

The investigation needs to be widened to include additional airfoil shapes, as the profiles in the 4-digits family have wider trailing edge angles than airfoils with the same thickness from other families (fig. 1); as well as that, throughout the NACA 4-digits family, the ratio of airfoil thickness over trailing edge angle shows only small variations.

To overcome such limitations, the investigated database is widened by modifying the thickness distribution, which is scaled with a half-cosine function aft the point of maximum thickness x_{thm}. The scaling function depends on an additional parameter k_{cos}:

$$\frac{t_{mod}}{t_{NACA}} = \begin{cases} 1 & for\ x \leq x_{thm} \\ 0.5 + 0.5\cos\left(\pi \frac{x - x_{thm}}{1 - x_{thm}}\ k_{cos}\right) & for\ x > x_{thm} \end{cases} . \tag{5}$$

The thickness modification allows for profiles with sharper trailing edges (figure 1), and introduces further variation in the dataset of investigated airfoil shapes.

2.2 Panel code simulation

The indicial response of each airfoil in the dataset is first obtained from panel code simulations. The code has been developed by Gaunaa[14], following Hess's formulation[18], where the singularity elements are given by: constant strength source distribution, constant strength vortex distributions, and two dimensional point vortices in the wake. A detailed description of the model, and its validation are presented in Gaunaa[14].

As previously mentioned, the unsteady aerodynamic forces in attached flow can be described as the sum of a non-circulatory (added mass), and a circulatory contribution. Von Karman and Sears [19] adopt a similar description in their study on unsteady aerodynamic forces of a thin airfoil undergoing motion, under the plane wake approximation. Von Karman and Sears further split the circulatory contribution in a quasi-steady and a wake memory part; the wake

[1] The original formulation for the thickness distribution function, presented in equation 2 in [17], returns non-zero thickness at the trailing edge. The original equation is here modified, by setting the coefficient $d_0 = 0$, in order to obtain zero-thickness at the airfoil trailing edge.

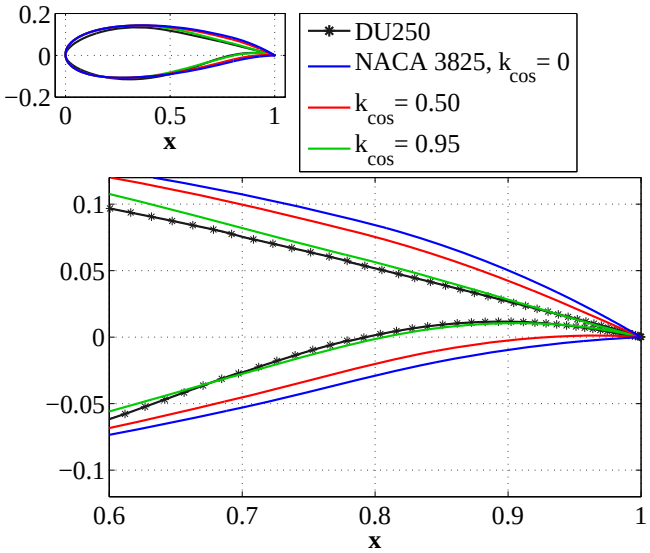

Figure 1: *Airfoil shapes and Trailing Edge angle. The NACA 3825 airfoil (blue line) has the same thickness and maximum camber as the DU91-W2-250 (black line), but a wider TE angle. The cosine thickness modification (red and green lines) yields to a sharper trailing edge.*

memory part represents the deficiency, with respect to the quasi-steady force, following a change in the airfoil quasi-steady loading, and, thereof, a change in the airfoil circulation. They show that the wake memory effects do not depend on how the change in quasi-steady loading is generated.

The same behavior is reported in the work by Gaunaa [20], where the aerodynamic forces due to arbitrary motion and deformation of an airfoil are derived under thin airfoil assumptions. Gaunaa shows that the quasi-steady loading of the airfoil can be represented by an equivalent three-quarters chord downwash $w_{3/4}$; the equivalent downwash $w_{3/4}$ encompasses, in a single term, all the sources of quasi-steady loading, as, for instance, the airfoil linear motion, the angle of attack and its angular rate, the camber-line deformation and its time derivatives. The wake memory effect depends directly on the change in the equivalent three-quarter chord downwash $w_{3/4}$, and not on which source has caused the change.

It can be thus concluded from thin airfoil analysis that the indicial response function accounting for the wake memory effects will be the same, independently of the cause of the step change in the quasi-steady loading (impulsively started flow, step in angle of attack, step in a trailing edge flap deflection, step in heave velocity, etc.); consequently, under the usual assumptions of thin airfoil theory, the circulatory indicial lift response function derived from an impulsively started flow is identical to the response function derived from a step change in angle of attack.

Furthermore, it is worth mentioning that the indicial lift response function for a step change in the airfoil quasi-steady loading differs from response

functions for disturbances traveling along the airfoil, as for instance the gust response function. Nevertheless, most aeroelastic simulation codes do not distinguish between step-change (Wagner-type response), and traveling disturbances (Küssner-type response), and a step change indicial response function is usually adopted in all the cases; an evaluation of the error introduced by this approximation is reported in Buhl et al.[21].

Based on the previous considerations and for practical purposes, it is chosen to perform panel code simulations of the indicial lift response by reproducing an impulsively started flow, where the free stream flow velocity is switched from zero to a finite value simultaneously in the whole computation domain. The indicial lift response function is then determined by letting the simulation advance in time, without further changes to the free stream speed. Preliminary computations have verified the validity of the assumption that, also for finite thickness airfoils, the circulatory lift response for an impulsively started flow matches the response following a step change in angle of attack.

By applying small time steps to the initial instants of the simulation, the panel code returns an unusual behavior of the indicial lift, which starts decreasing from a value above the steady one. Such results are similar to the transient behavior described by Graham [22] for an airfoil in impulsively started flow where the roll up of wake vorticity dominates the unsteady aerodynamics. In these conditions, the indicial lift presents an initial singularity: it first decreases with time, and only subsequently monotonically increases, as in Wagner's indicial response function.

As observed by Graham, an airfoil does not encounter a truly impulsive start under realistic conditions. The wake dynamic is thus generally dominated by downstream convection of the vorticity, rather than roll up, and the indicial lift increases monotonically to the steady value. The present investigation focuses on the response of airfoils under realistic conditions, therefore, time steps are selected as large as sufficient to avoid the singularity induced by the dynamics associated with the rolling up of the initial part of the shed wake vortex sheet. The response at time zero is then obtained from a quadratic extrapolation of the first computed points.

2.3 Exponential curve fitting

The simulated indicial response can be approximated by a n-term exponential function, eq. (3); the more terms, the better the approximation. It is chosen to use a two-term function, which returns a sufficiently accurate approximation (figure 3) and keeps similarity with Jones's expression:

$$\Phi = 1 - A_1 \exp^{b_1 \cdot \tau} - A_2 \exp^{b_2 \cdot \tau}, \tag{6}$$

with: $b_1 < b_2 < 0$.

The two-term function is defined by 4 *indicial response coefficients*: b_1 giving the decay of the fast term, b_2 for the slow decaying term, and A_1 and A_2 giving the weights of the two components. The coefficients are found through minimization of the weighted sum of the squared differences between the simulated response and the fitted curve.

The weight function is set to be equal to the difference between the simulated indicial response, and the steady value. In this way, the minimization algorithm

values more the fitting for points in the initial part of the transient, reducing the influence from the almost stationary tail of the indicial curve; for the same purpose, the curve tail is truncated where the response reaches 99.9% of the final value.

2.4 Profile Surface Angle

A preliminary investigation indicates that the lift response coefficients are related to the angle between upper and lower surface of the profile, especially close to the trailing edge, as was also observed in Chow[13].

It is therefore chosen to represent the geometric characteristics of an airfoil in terms of a *profile surface angle* $\beta(x)$. For a given chord-wise coordinate $\tilde{x}$, $\beta(\tilde{x})$ is defined as the angle between two lines that originate at the trailing edge and intersect the profile upper and lower surface at the points of chord-wise coordinate $\tilde{x}$, figure 2.

Each airfoil is thus characterized by a specific curve $\beta(x)$ of profile angles along the chord; the same airfoil is also associated to a set of indicial response coefficients (A_1,A_2,b_1,b_2). Therefore, a relation between the indicial response coefficients and the angles β would allow to estimate the indicial lift response function of an airfoil from simple measurement of its geometric characteristics.

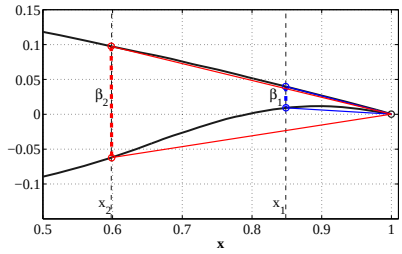

Figure 2: *Profile angle β at chord-wise position x_1 and x_2*

3 Results

A preliminary investigation is carried out on simple airfoils shapes from the NACA 4-digits family. It is observed that the indicial lift response function is scarcely influenced from variations of airfoil camber and leading edge radius; on the contrary, the airfoil thickness and the location of the point of maximum thickness affect the shape of the indicial response function. As also observed in Gaunaa[14] and Chow [13], thicker airfoils have a slower response and the indicial lift response functions have a starting value below the $\Phi_{(\tau=0)} = 0.5$ value of the flat plate; as the airfoil thickness is reduced, the response tends to the flat plate one, figure 3.

The investigation is then enlarged to a wider dataset of airfoil profiles, including several combinations of airfoil thickness and cosine scaling parameter. For each profile in the dataset, the panel code simulates the indicial lift response,

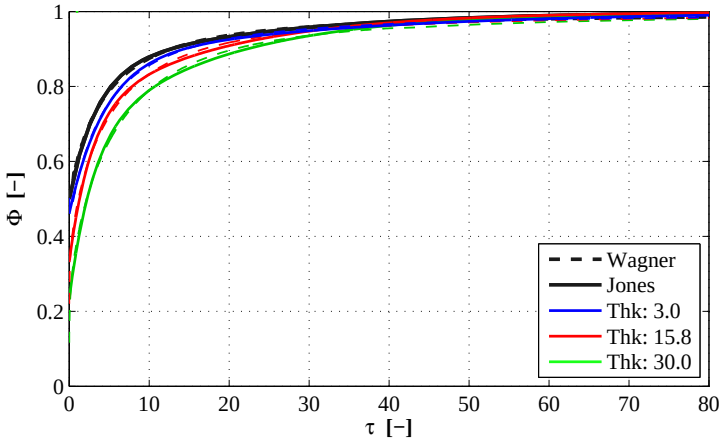

Figure 3: *Indicial lift response function for NACA 44xx airfoils with different thicknesses, and for a flat plate with Jones's approximation (full black line) and Wagner's response function (dashed black line). Dashed color lines: response simulated by the panel code; full lines: two terms exponential approximation.*

which is then fitted with the two terms approximation; every airfoil profile i is thus associated with a set of four indicial response coefficients (A_1^i, A_2^i, b_1^i, b_2^i, as in eq. (6)), and a set of profile angles measured at different chord-wise locations: $\beta(x)_i$. A relation is sought between the indicial response coefficients and the profile angle at few selected locations.

At first, it is assumed that each of the four indicial response coefficients can be expressed as a quadratic function of the profile angle measured at one single chordwise location x_1:

$$\hat{y} = a_0 + a_1\beta_{x1} + a_2\beta_{x1}^2 \ , \qquad \text{where} \qquad \hat{y} = \hat{A}_1,\ \hat{A}_2,\ \hat{b}_1,\ \text{or}\ \hat{b}_2. \tag{7}$$

The problem is formulated as a linear model regression, where, for each profile i, the actual value of the indicial response coefficient $\zeta_{i,1}$ ($\zeta_{i,1} = A_1^i$, A_2^i, b_1^i, or b_2^i) is the dependent variable (regressand), and the profile angle at a selected location $\beta(\tilde{x})_i$ is the independent variable (regressor). The regression parameters a_0, a_1, a_2 are constant throughout the dataset, and a different set of regression parameters is associated to each indicial response coefficient.

The problem is solved with an ordinary least square method, minimizing the squared sum of residuals $(\hat{y}_i - \zeta_{i,1})^2$; the regression is repeated considering different locations $\tilde{x}$ of the profile angle measurement point.

For each chord-wise location $\tilde{x}$, the quality of the regression is evaluated by the coefficient of determination $r^2(\tilde{x})$; the minimum points of the curves $(1-r^2)$ (figure 4, top) thus indicate the optimal locations x^*: the corresponding profile angles $\beta(x^*)$ give the regression with the best explanation of the variation observed in the indicial response coefficients.

Although optimally placed, measurements of the profile angle at only one point are not sufficient to account for all the variation observed in the indicial response coefficients. A profile angle measured in a second point x_2 is thus introduced in the empirical function: $\hat{y} = f\,(\beta_{x1}, \beta_{x2})$.

The optimal location of the second point is determined from the coefficient

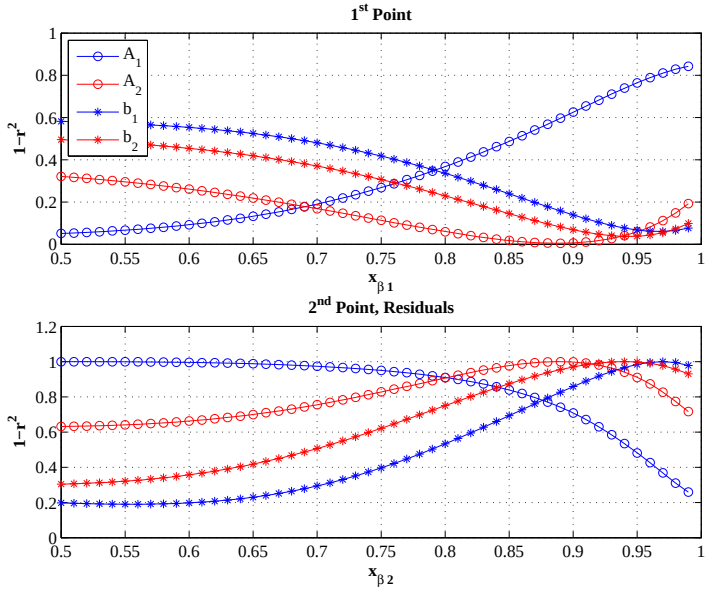

Figure 4: *One minus the coefficient of determination versus the location of the profile angle measurement point; the curves minima correspond to the best regression. Top: location of the first profile-angle point x_1, regression on the dataset. Bottom: location of the second profile-angle point x_2, regression on the residuals.*

of determination r^2 in a second regression, where the regressand variables $\zeta_{i,2}$ are the residuals from the first regression: $\zeta_{i,2} = \hat{y}_{i,1} - \zeta_{i,1}$. The minima of the $(1 - r^2)$ curves (figure 4, bottom) give the optimal placement for the second profile angle measurement β_{x2}. Note that, since the second regression (figure 4, bottom) fits the residuals of the first, whenever the second measurement point x_2 coincides with the first x_1, the coefficient $(1 - r^2)$ is one, which indicates that the second point, being identical to the first, does not contribute to further data explanation.

The regression analysis indicates for each indicial response coefficient the optimal locations of the two measurements points for the profile angle. The optimal locations are slightly moved from the curves minima so to reduce the total number of points to 3; the resulting pair of measurement points are reported in the first columns of table 1. For each indicial response coefficient, one point is located close to the airfoil trailing edge, the other to mid-chord; thus indicating that the geometric parameters that more affects the indicial lift response function are the airfoil thickness (roughly proportional to the profile angle at mid-chord), and the profile 'opening' near the trailing edge.

Each indicial response coefficient is then estimated as a quadratic function of the profile angle β at the two selected locations (x_1 and x_2) along the profile:

$$\hat{y}_i = a_0 + a_{11}\beta_{x1} + a_{12}\beta_{x1}^2 + a_{21}\beta_{x2} + a_{22}\beta_{x2}^2. \tag{8}$$

Both the profile angle location pair (x_1 and x_2), and the set of regression parameters a_i depend on which of the four indicial response coefficient is being considered: $\hat{y}_i = \hat{A}_1, \hat{A}_2, \hat{b}_1$, or $\hat{b}_2$ (table 1); the regression parameters are again determined by solving a least square regression problem.

Table 1 reports the profile angle location and the regression parameters for each indicial response coefficient. The parameters for the quadratic terms (a_{12},a_{22}) are rather close to zero, highlighting a dominant linear behavior; nevertheless, no regression parameter admits the zero value inside its 95% confidence interval, thus also the quadratic terms are significant in the fitting. Substituting the sets of regression parameters in equation (8) yields to a set of four empirical equations, one for each indicial response coefficient; the equations allow to estimate the indicial lift response function of an arbitrary profile by simply measuring its profile angle in three different locations.

Lift Coef.	x_1	x_2	a_0	a_{11}	a_{12}	a_{21}	a_{22}
A_1	0.95	0.5	3.93E-01	-1.32E-03	3.41E-05	2.06E-05	5.33E-05
A_2	0.88	0.5	1.01E-01	9.41E-03	-7.80E-05	2.35E-03	-9.24E-05
b_1	0.95	0.5	-1.90E-01	-8.35E-03	1.04E-04	-7.16E-03	2.65E-04
b_2	0.95	0.5	-2.83E-02	-1.29E-03	1.85E-05	-1.04E-03	3.44E-05

Table 1: *Empirical estimation of the indicial lift response coefficients. Location of the two profile angle measurement points: x_1, x_2. Regression parameters to be applied in equation* (8) *for coefficient estimation; the parameters refer to profile angles measured in degrees.*

3.1 Validation

The set of empirical equations derived in the previous section is tested for three airfoil profiles used on the reference rotor of the MEXICO project[23]: DU 91-W2-250, RISOE A1-21, and NACA 64-418. The airfoils have profile shapes commonly employed on wind turbine blades, they differ in thickness and camber characteristics, and none of them was part of the dataset used in the regression.

For each airfoil, the indicial lift response coefficients are estimated with the empirical relation in eq. (8), and the coefficients in table 1 (circles, in figure 5); the indicial response coefficients are then compared with the coefficients resulting from the direct fitting of the indicial lift response function simulated by the panel code (stars). The estimated values are very close to the panel codes ones, and they give a better approximation of the indicial lift response than Jones's coefficients.

The empirical equations are further tested to verify that plausible lift response functions are obtained for profile angles ranges:

$$\forall \text{ profile } \begin{cases} 2^\circ \leq & \beta_{x1} & \leq 50^\circ \\ 3^\circ \leq & \beta_{x2} & \leq 40^\circ \end{cases} . \tag{9}$$

The empirical equation might result in an unreasonable indicial lift response when applied to airfoils falling outside this range.

4 Relevance to Aeroelastic Simulations

4.1 CFD comparison

Changing the indicial lift response function conditions the dynamics of the aerodynamic forces. The effects are first evaluated in the simple case of a 2D airfoil undergoing harmonic pitching motion. The same three airfoil profiles as in

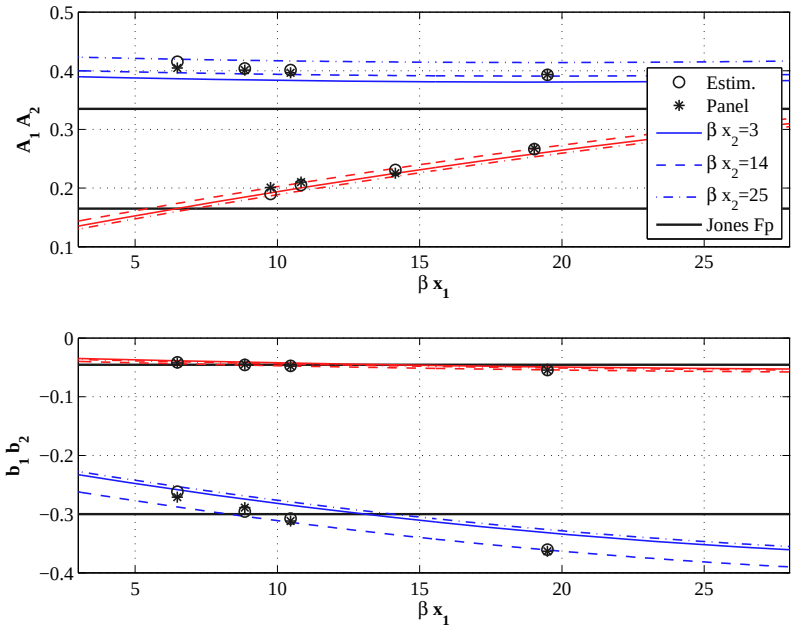

Figure 5: *Lift response coefficients as function of the airfoil profile angle at location x_1. Estimated (circles) and panel code (stars) coefficients for the airfoils: DU 91-W2-250, RISOE A1-21, NACA 64-418 (from the left). The plot reports curves from the empirical estimation function for three arbitrary β_{x2} profile angles, and the flat plate coefficients from Jones's approximation.*

the previous validation are considered; the profiles are hinged at the quarter chord point, and the angle of attack is changed from 1° to 3° with two reduced frequencies: $k = \omega b/U = 0.1$, and a faster one $k = 0.5$.

The unsteady lift force is computed with the analytical model described in Hansen et al.[4]; the model, here simplified for attached flow conditions, is based on superposition of indicial lift response functions approximated by exponential terms. For each airfoil, three sets of indicial response coefficients are considered: the ones from Jones's flat plate expression, the estimations from the empirical equation, eq.8, and the ones obtained by exponential fitting of the panel code response.

The resulting lift loops (figure 6) are compared against CFD simulations. The CFD results were obtained using EllipSys, Risø's in-house CFD code, developed as a cooperation between the Department of Mechanical Engineering at the Technical University of Denmark and the Department of Wind Energy at Risø National Laboratory [24, 25, 26]. Simulations are run with a standard set-up for 2D airfoils: fully turbulent flow, k-ω SST (Shear Stress Transport) turbulence model, and Reynolds number of 6 millions.

The estimated indicial response coefficients are very close to the panel code ones (see figure 5): the corresponding loops (respectively, blue line and red circles in figure 6) are thus practically overlapping. The loops based on the estimated indicial response coefficients are closer to the CFD results (black lines)

than the loops with flat plate coefficients, indicating thus a better approximation of the airfoil indicial lift response function. The differences among the loops increase as the reduced frequency is augmented.

4.2 Full Wind Turbine Simulations

In most aeroelastic codes for wind turbine loads simulation, the indicial response coefficients are given by Jones's approximation of the flat plate response. As observed in the previous sections, the response of an airfoil with finite thickness differs from the flat plate one, and the higher is the reduced frequency of the unsteady motion, the larger the difference in the resulting aerodynamic forces.

To assess the impact of differences in the indicial lift response function on the simulated response of a full wind turbine, the NREL offshore 5-MW baseline wind turbine [15] is modeled with the aeroelastic tool HAWC2[3]. Three different set-ups of the aerodynamic model are considered in the simulations, where the indicial response coefficients are given by:

- Jones's flat plate response. The default value in most aeroelastic simulation tools.
- Estimated coefficients for the DU 91-W2-250 airfoil. The airfoil has a thickness ratio of 25%, suitable for mid-span sections. The current version of the aeroelastic tool does not allow to variate the indicial lift response coefficients along the blade span, therefore, the DU 91-W2-250 indicial response approximation is applied to the whole blade.
- Quasi-Steady approximation ($A_1 = A_2 = 0$) for the circulatory lift contribution in attached flow; also a rather common assumption.

The effects of the different indicial response approximations on aeroelastic simulations are quantified in terms of variations of equivalent fatigue loads, ultimate loads, and stability limits.

4.2.1 Fatigue and Ultimate Loads

The equivalent fatigue loads are determined using a standard procedure [27] based on rain flow counting method, and Palmgren-Miner linear damage assumption. The simulations reproduce power production load cases as described in the IEC standard 61400-1 [28] (DLC 1.1); wind conditions for turbine class *IIb* are adopted, and a yaw misalignment of $\pm 8^\circ$ is included. The stochastic wind field is reproduced through Mann's turbulence model [3], and the same turbulence seeds are repeated for the three indicial response set-ups.

The ultimate loads are computed as the maximum load among a reduced set of simulation cases from the same standard [28]: production with extreme turbulence model (DLC 1.3), extreme coherent gust (DLC 1.4), and extreme operating gust (DLC 2.3) without grid-loss.

Table 2 and 3 report the variation in simulated equivalent fatigue loads and ultimate loads for bending moments measured at the blade root, and at the tower bottom flange, and torsion moments at the tower top, and on the low speed shaft; the loads variations are normalized by the loads obtained with the default flat plate indicial response coefficients.

Although the figures might vary depending on the specific wind turbine and control model, it can be concluded that the assumption of quasi-steady circulatory lift in attached flow leads to significantly higher estimations of both fatigue and ultimate loads. Using the finite-thickness indicial lift response function leads to a reduction in the predicted loads, in comparison with simulation based on a flat-plate indicial response, but the variations are on a much smaller scale than in the quasi-steady case.

S_{eq}	*Blade Flapw.*	*Blade Edgew.*	*Blade Tors.*	*Tower FA*	*Tower SS*	*Tower Tors.*	*Shaft Tors.*
Ref. Fl.Pl. [MNm]	13.73	10.69	0.25	77.12	39.55	20.60	3.86
Δ *Quasi-St*	5.49 %	1.10 %	20.54 %	6.44 %	3.89 %	9.15 %	15.05 %
Δ *DU 250*	-1.06 %	0.00 %	-2.48 %	-1.02 %	-0.39 %	-1.83 %	-2.21 %

Table 2: *Equivalent fatigue loads, variations due to changes of the indicial lift response coefficients. Simulations for: Jones's flat plate indicial response coefficients (reference case, first row), Quasi-Steady indicial response, DU 91-W2-250 indicial response coefficients; variations Δ normalized by the equivalent loads of the flat plate reference case. Results refer to an equivalent number of load cycles $n_{eq} = 10^6$, material fatigue exponent $m = 10$ for blade loads, $m = 4$ for tower and drive-train.*

$\max(\lvert M \rvert)$	*Blade Flapw.*	*Blade Edgew.*	*Blade Tors.*	*Tower FA*	*Tower SS*	*Tower Tors.*	*Shaft Tors.*
Ref. Fl.Pl. [MNm]	14.94	6.92	0.22	112.46	45.08	17.44	6.62
Δ *Quasi-St.*	6.93 %	2.29 %	25.26 %	-1.98 %	3.44 %	6.07 %	5.45 %
Δ *DU 250*	-0.73 %	-0.39 %	-2.21 %	0.41 %	-0.55 %	-1.14 %	-1.33 %

Table 3: *Ultimate loads from reduced set of cases, variations due to changes of the indicial lift response coefficients. Simulations for: Jones's flat plate indicial response coefficients (reference case, first row), Quasi-Steady indicial response, DU 91-W2-250 indicial response coefficients; variations Δ normalized by the ultimate loads of the flat plate reference case.*

4.2.2 Stability limits

The wind turbine stability limits in the three indicial response cases are estimated by running simulations with a constant wind inflow, and attached flow conditions on the blades. The rotor speed is progressively increased until unstable oscillations are observed. The results are presented in figure 7 as the tip speed corresponding to the critical rotor speed at which instability occurred; the torsional stiffness of the blade has been scaled (values on the abscissa) to verify the consistency of the results for different stiffness values.

As discussed for fatigue and ultimate loads, neglecting the circulatory lift dynamics in attached flow causes the largest variations in the simulated response. The stability limit encountered with the quasi-steady assumption is in fact much lower than in the other two cases; Lobitz [29] reported a similar result for the flutter limit of an isolated blade. The finite-thickness indicial lift response function results in slightly higher stability limits, but the difference from the flat plate case is rather small; variations of similar magnitude were reported in the flutter analysis of a 2D profile [30].

As discussed in Hansen [31], the increased flutter limits returned by the flat plate and the thick airfoil responses are qualitatively explained by the respective effective lift curves, figure 6. In fact, the effective lift slope returned by the finite-thickness response (blue lines in figure 6) is slightly milder than the flat-plate one (green lines), which is in turn much less steep than the quasi-steady one (dashed lines).

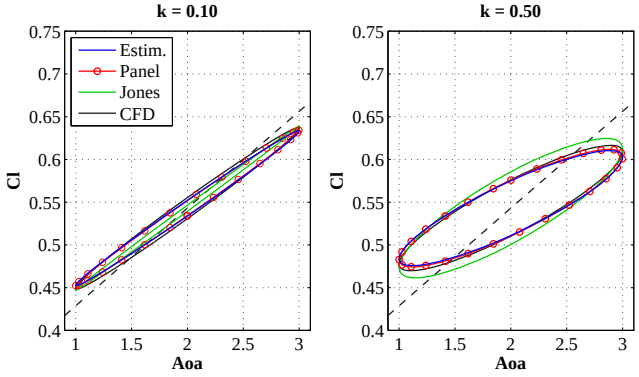

(a) NACA 64-418.

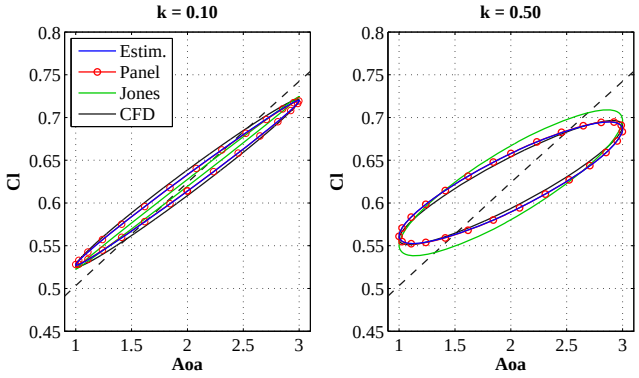

(b) DU 91-W2-250.

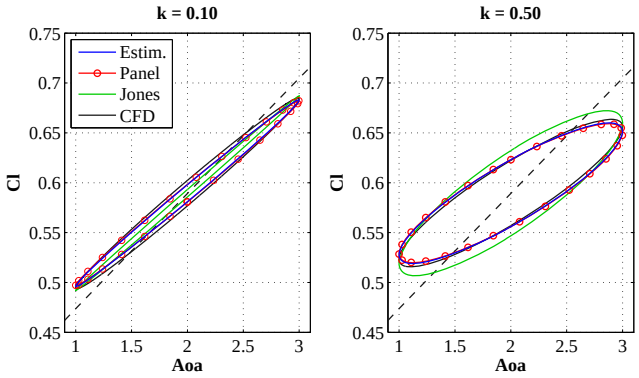

(c) RISOE A1-21.

Figure 6: *Lift coefficient loops for airfoils undergoing harmonic pitching motion. Comparison between CFD results (black) and analytical model based on indicial response coefficients from: empirical estimation function (blue), panel code response (red line with circles), Jones's flat plate coefficients (green).*

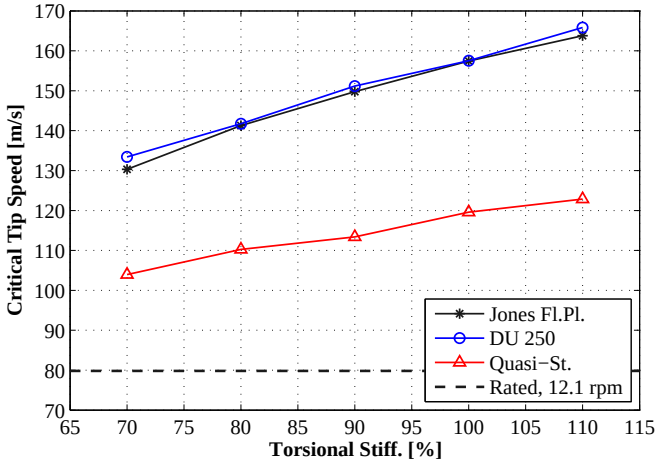

Figure 7: *Critical tip speed at which instability (flutter) due to rotor over-speeding arises; variations due to changes of the indicial lift response coefficients. Simulations for: Jones's flat plate indicial response coefficients (black with stars), Quasi-Steady indicial response (red with triangles), DU 91-W2-250 indicial response coefficients (blue with circles). The values are plotted versus the scaling factor applied to the blade torsional stiffness.*

5 Conclusion

Airfoils with finite-thickness have an indicial lift response function that is different from the flat plate one, which is usually adopted in aeroelastic simulations through Jones's approximation.

The indicial response of several airfoil shapes is determined using a panel code, and then approximated by a two-term exponential function; the exponential function is similar to Jones's expression for the flat plate, and is defined by four indicial response coefficients, eq. (6).

An empirical relation is proposed, where the four indicial response coefficients are estimated by quadratic functions of the airfoil profile angles, measured at three locations along the chord. The relation allows to estimate the indicial lift response function of a finite-thickness airfoil from simple geometric characteristics.

The indicial response function conditions the dynamics of the simulated unsteady aerodynamic forces. The effects are evident in the case of a 2D airfoil undergoing harmonic pitching motion, where the indicial response accounting for the thickness of the airfoil leads to a better agreement with results from CFD simulations.

The effects of different indicial response approximations on the overall estimation of the wind turbine aeroelastic behavior are quantified for the NREL 5-MW baseline turbine [15]. The quasi-steady response function has a significant impact on the simulated turbine response: fatigue and ultimate loads are larger, and the stability limits lower, than the corresponding values obtained with a flat-plate indicial response. The indicial response function that accounts for the airfoil thickness, in comparison to Jones's flat-plate indicial response, leads to a slight reduction of the aeroelastic loads, and a small increase of flutter stability limits; although the variations from the default flat-plate case are small.

To conclude, an aerodynamic model for aeroelastic simulations should account for the dynamics of the circulatory lift, also in the attached flow region, as a quasi-steady approximation results in heavily biased loads and stability estimations. The aerodynamic model based on the indicial response function that accounts for the airfoil thickness yields more accurate predictions of the aerodynamic forces than the model using Jones's flat-plate indicial response. However, the improvement given by the finite-thickness indicial response over the flat plate approximation is scarcely noticeable when the aeroelastic behavior of the whole wind turbine is considered.

6 Acknowledgments

It is gratefully acknowledged that this work is partly funded by the Danish project *Development of Adaptive Trailing Edge Flap (ATEF) System for Wind Turbines* by the Advanced Technology Foundation, Advanced Technology Projects 2007.

References

[1] Beddoes TS. Practical computations of unsteady lift. *Vertica* 1984; **8**(1):55–71.

[2] Leishman JG, Nguyen KQ. State-space representation of unsteady airfoil behavior. *AIAA Journal* 1990; **28**(5):836–844.

[3] Larsen TJ. How 2 HAWC2 the user's manual. *Technical Report R-1597(EN)*, Risø National Laboratory. Technical University of Denmark 2009.

[4] Hansen MH, Gaunaa M, Madsen HA. A Beddoes-Leishman type dynamic stall model in state-space and indicial formulations. *Technical Report R-1354(EN)*, Risø National Laboratory, Roskilde (DK) 2004.

[5] Bossanyi E. GH Bladed theory manual. *Technical Report*, Garrad Hassan and Partners Ltd 2003.

[6] Jonkman JM, Buhl MLJ. Fast user's guide - updated august 2005. *Technical Report NREL/TP-500-38230*, National Renewable Energy Laboratory (NREL) 2005.

[7] Moriarty PJ, Hansen AC. Aerodyn theory manual. *Technical Report NREL/TP-500-36881*, National Renewable Energy Laboratory (NREL) 2005.

[8] Theodorsen T. General theory of aerodynamic instability and mechanism of flutter. *Technical Report 496*, National Advisory Committee for Aeronautics (United States Advisory Committee for Aeronautics) 1935.

[9] Bisplinghoff RL, Ashley H, Halfman RL. *Aeroelasticity*. Dover Pubblications, Inc, 1996.

[10] Jones RT. The unsteady lift of a wing of finite aspect ratio. *Technical Report 681*, National Advisory Committee for Aeronautics (United States Advisory Committee for Aeronautics) 1940.

[11] Giesing JP. Nonlinear two-dimensional unsteady potential flow with lift. *Journal of Aircraft* 1968; **5**:135–143.

[12] Basu BC, Hancock GJ. Unsteady motion of a two-dimensional aerofoil in incompressible inviscid flow. *Journal of Fluid Mechanics* 1978; **87**(JUL):159–178.

[13] Chow CY, Huang MK. The initial lift and drag of an impulsively started airfoil of finite thickness. *Journal of Fluid Mechanics* 1982; **118**(MAY):393–409.

[14] Gaunaa M. Unsteady aerodynamic forces on NACA 0015 airfoil in harmonic translatory motion. PhD Thesis, Department of Mechanical Engineering, Technical University of Denmark 2002.

[15] Jonkman J, Butterfield S, Musial W, Scott G. Definition of a 5-MW reference wind turbine for offshore system development. *Technical Report NREL/TP-500-38060*, National Renewable Energy Laboratory (NREL) Feb 2009.

[16] Gaunaa M, Bergami L, Heinz J. Indicial response function for finite-thickness airfoils, a semi-empirical approach. *Conference proceedings, 49th AIAA Aerospace Sciences Meeting*, Orlando (FL), 2011.

[17] Stack J, Doenhoff AEV. Tests of 16 related airfoils at high speed. *Technical Report NACA-TR-492*, National Advisory Committee for Aeronautics (United States Advisory Committee for Aeronautics) 1935.

[18] Hess J. Higher order numerical solution of the integral equation for the two-dimensional Neumann problem. *Computer Methods in Applied Mechanics and Engineering* 1973; **2**(1):1–15.

[19] Karman T, Sears WR. Airfoil theory for non-uniform motion. *Journal of the Aeronautical Sciences* 1938; **5**(10):379–390.

[20] Gaunaa M. Unsteady two-dimensional potential-flow model for thin variable geometry airfoils. *Wind Energy* 2010; **13**(2-3):167–192.

[21] Buhl T, Gaunaa M, Bak C. Potential load reduction using airfoils with variable trailing edge geometry. *Transactions of the ASME.Journal of Solar Energy Engineering* 2005; **127**(4):503–516.

[22] Graham JMR. The lift on an aerofoil in starting flow. *Journal of Fluid Mechanics* 1983; **133**(AUG):413–425.

[23] Snel H, Schepers JG, Montgomerie B. The MEXICO project (Model experiments in controlled conditions): The database and first results of data processing and interpretation. *Journal of Physics: Conference Series*, vol. 75, 2007; 012 014.

[24] Michelsen JA. Block structured multigrid solution of 2D and 3D elliptic PDE's. *Technical Report AFM 94-06*, Technical University of Denmark 1994.

[25] Michelsen JA. Basis3D - a platform for development of multiblock PDE solvers. *Technical Report AFM 92-05*, Technical University of Denmark 1992.

[26] Sørensen NN. General purpose flow solver applied to flow over hills. *Technical Report Risø-R-827(EN)*, Risø National Laboratory 1995.

[27] Hansen M. *Aerodynamics of wind turbines : rotors, loads and structure*. James & James: London, 2000.

[28] IEC. IEC 61400-1: Wind turbines part 1: Design requirements. *Technical Report*, International Electrotechnical Commission 2005.

[29] Lobitz DW. Aeroelastic stability predictions for a MW-sized blade. *Wind Energy* 2004; **7**(3):211–224.

[30] Bergami L, Gaunaa M. Stability investigation of an airfoil section with active flap control. *Wind Energy* 2010; **13**(2-3):151–166.

[31] Hansen MH. Aeroelastic instability problems for wind turbines. *Wind Energy* 2007; **10**(6):551–577. Journal Article.